Microelectronics Reliability 121 (2021) 114119

Contents lists available at ScienceDirect

Microelectronics Reliability

journal homepage: www.elsevier.com/locate/microrel

Automated abstraction of nonlinear analog circuits to reliable set-valued models with reduced overapproximation

Malgorzata Rechmal-Lesse *, Yeremia Gunawan Adhisantoso, Gerald Alexander Koroa, Markus Olbrich

Institute of Microelectronic Systems, Leibniz University Hannover, Germany

ARTICLE INFO

Keywords:
Nonlinear analog circuit
Piecewise linear model
Formal verification
Reachability analysis
Parameter variations

ABSTRACT

This paper tackles the analog and mixed-signal modeling for verification challenges. It proposes an adjustable automated modeling approach, which provides set-valued models with reduced overapproximation. The models reliably enclose parameter variations and modeling errors. The reduced overapproximation is obtained by computing the intersecting set of models with intervals and affine forms. The nonlinear circuit examples show a reduced overapproximation up to 86%.

1. Introduction

Reliability of integrated circuits becomes increasingly challenging with the ongoing trend of miniaturization. Even small uncertainties can lead to a circuit's failure. Verification methods are applied for proving correct behavior. Developers are confronted with many difficulties with common verification methods. Simulation runs only provide limited reliability, since a complete coverage of the parameter space is not possible in finite time. There are several approaches to cover parameter variations and modeling errors with range arithmetic [1–3]. The drawback of using ranges is unnecessarily conservative overapproximation. Models that reliably enclose all uncertainties and perform the enclosure as close as possible to cover the simulation results are desirable.

Complex integration among analog/digital designs in a single chip is another challenge. In the digital domain formal verification on system-level is established. In the analog domain verification relies on transistor-level simulation and experience. Verifying digital and analog parts independently is error-prone. The proper interaction of all parts has to be guaranteed. Another possible source of error is the generation of the models manually. Therefore, automated approaches are preferable.

Modeling analog and mixed-signal circuits (AMS) as hybrid automata (HA) and verification with reachability analysis offer promising solutions [4–6]. Modeling of AMS circuits with hybrid automata provides the advantage of preserving the discrete and continuous behavior in a common system. With reachability analysis it is possible to determine the set of all reachable states, starting from a set of initial states under the influence of a set of inputs and disturbances. The possibility to include variations as additive terms is described in [7,8]. A significant enhancement was presented in [9]. In contrast to previous methods, this approach enables to model parametric variations in individual components with intervals and affine forms.

In this paper, we elaborate on the findings of our previous work [9]. Shortly summarizing, we have presented an approach for providing reliable models of nonlinear analog circuits for formal verification. We have shown that modeling with affine forms do not generally result in lower overapproximation than modeling with intervals. To reduce the generated overapproximation we suggested to consider only the intersecting set of the resulting sets modeled with different methods.

In this paper, we pursue the approach to reduce the overapproximation. We refine it for automation and generate an optimized model for each example. Moreover, we prove the applicability to highly nonlinear circuits and provide analyses around the stable point under the influence of variations and disturbances.

The remainder of this paper is organized as follows. In Section 2 we describe the modeling framework. Then we present the reduction of the overapproximation in Section 3. Finally, we provide results in Section 4 and conclude this paper in Section 5.

* Corresponding author.
E-mail addresses: malgorzata.rechmal@ims.uni-hannover.de (M. Rechmal-Lesse), yeremia.gunawan@ims.uni-hannover.de (Y.G. Adhisantoso), gerald.koroa@ims.uni-hannover.de (G.A. Koroa), markus.olbrich@ims.uni-hannover.de (M. Olbrich).

https://doi.org/10.1016/j.microrel.2021.114119
Received 13 October 2020; Received in revised form 26 February 2021; Accepted 30 March 2021
Available online 23 April 2021

2. Modeling framework for parametric variation

In this section, we describe the automated approach for generation of set-valued models, presented in [9]. It is divided into the generation of symbolic circuit models, modeling of parameter variations with range arithmetic and the inclusion of these models in the modeling framework. Fig. 1 gives an overview of the framework.

2.1. Automated generation of symbolic circuit models

For the automated generation of symbolic circuit models a circuit netlist and piecewise linear (PWL) models of all nonlinear devices are required. The PWL modeling is based on [10]. PWL models are obtained from detailed SPICE reference models. The reference models are finely sampled to gain data points. Following, linear regions from these data points are constructed. For this purpose the change point detection algorithm [11] for devices like diodes or the Delaunay triangulation for devices with more than one input like transistors are applied. The number of linearized regions is adjustable for finding a tradeoff between model complexity and accuracy. As described in [9], the increasing PWL granularity boosts the unnecessarily conservative overapproximation. Using optimization techniques like simulated annealing or genetic algorithms the linear regions are minimized.

In the next step, the nonlinear devices are replaced with the PWL models and represented as controlled sources and passive components. The netlist is converted into system equations by using the Modified Nodal Analysis [12].

$$\begin{aligned}(s\mathbf{C}_0 + \mathbf{G}_0)\mathbf{x}_0 &= \mathbf{B}_0\mathbf{u}\\ \mathbf{y}_0 &= \mathbf{D}_0\mathbf{x}_0\end{aligned} \tag{1}$$

with $\mathbf{C}_0$ and $\mathbf{G}_0$ as inductance/capacitance and conductance matrices, $\mathbf{x}_0$ as a state vector and the product of $\mathbf{B}_0\mathbf{u}$ as a vector of independent sources. The product of $\mathbf{D}_0\mathbf{x}_0$ is the output vector.

All passive components in these matrices are represented by symbolic variables $\widetilde{R}$, $\widetilde{C}$ and $\widetilde{L}$. In this paper, symbolic variables are denoted by ($\widetilde{\ }$). For example, in case of the two stage nonlinear transmission line in Fig. 3(b), $\mathbf{G}_0$ results in

$$\mathbf{G}_0 = \begin{bmatrix} \frac{1}{\widetilde{R}_0}+\frac{1}{\widetilde{R}_1} & -\frac{1}{\widetilde{R}_1} & 0 & 1 \\ -\frac{1}{\widetilde{R}_1} & \frac{1}{\widetilde{R}_1}+\frac{1}{\widetilde{R}_2}+\frac{1}{\widetilde{R}_{D_1}} & -\frac{1}{\widetilde{R}_2} & 0 \\ 0 & -\frac{1}{\widetilde{R}_2} & \frac{1}{\widetilde{R}_2}+\frac{1}{\widetilde{R}_{D_2}} & 0 \\ 1 & 0 & 0 & 0 \end{bmatrix} \tag{2}$$

The system equations are transformed to state-space representation based on [13]. State-space models at block-level are composed from the device models previously obtained. The compositional approach promotes exponential growth of the number of linear regions. This problem

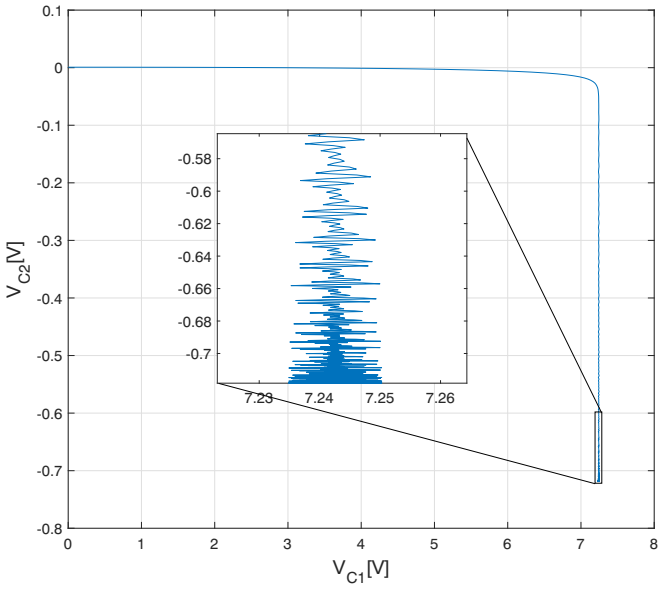

Fig. 2. Simulation of the circuit LPF.

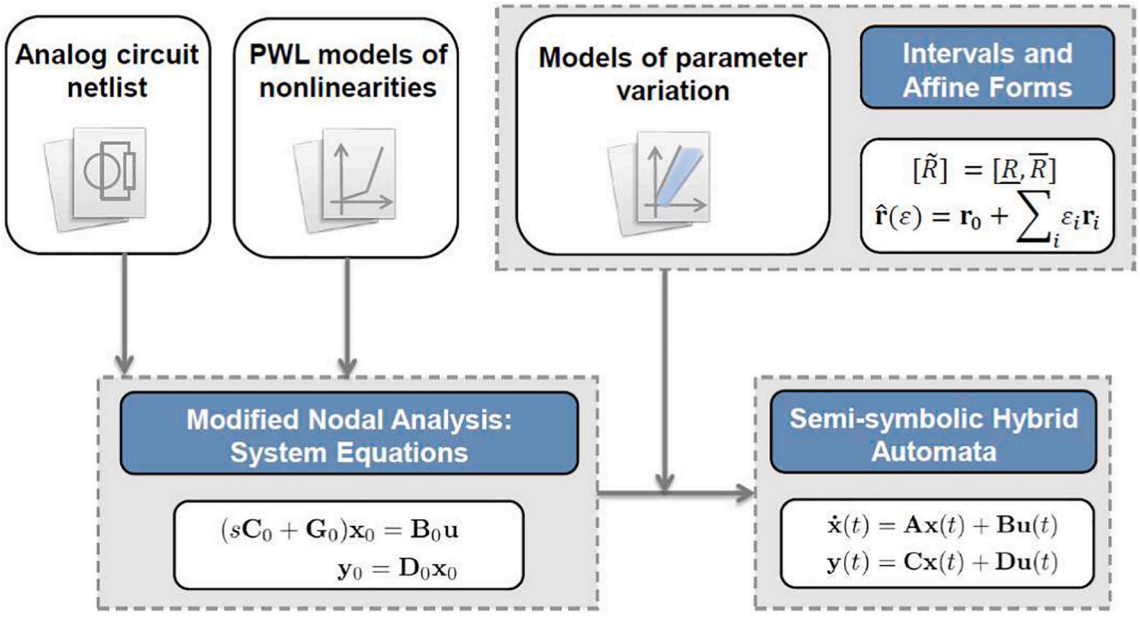

Fig. 1. Modeling framework for parametric variation.

is avoided by providing reachable region combinations on demand, according to [14,15]. Only regions that are reachable from previously reached regions are computed.

2.2. Modeling parameter variations with range arithmetic

Reliable modeling of uncertainties like process variations, drift, aging, noise requires set-valued models. For this purpose we use range arithmetic, more precisely intervals and affine forms.

The definition of an interval $[x]$ is a set of real numbers

$$[x] = \left[\underline{x}, \overline{x}\right] = \left\{x \in \mathbb{R} | \underline{x} \leq x \leq \overline{x}\right\} \tag{3}$$

bounded by $\underline{x}$ as minimum and $\overline{x}$ as maximum.

Affine arithmetic represents intervals as symmetric sums, called affine forms,

$$\hat{x} = x_0 + \sum_i \varepsilon_i x_i \text{ with } \varepsilon_i \in [-1; 1] \tag{4}$$

with x_0 as the center value, ε_i as the noise symbols and $x_i \in \mathbb{R}$ as the partial deviations. In this paper affine forms are denoted by $\hat{(\,)}$. Every ε_i describes the influence of an uncertainty on $\hat{x}$ and might accept a real value within the given bounds $[-1; 1]$. The partial deviations x_i are given by the size of the uncertainty.

Mathematical operations on affine forms result in a new affine form. Linear operations provide exact results and do not generate further deviation terms. On the other hand, nonlinear operations introduce new deviation terms describing the approximation error [16].

2.3. Inclusion of parameter variation models

In the resulting matrices all symbolic variables are substituted with intervals and affine forms, respectively. Exemplary a resistor $\widetilde{R}$ is replaced with its model of parameter variation $\left[\widetilde{R}\right] = \left[\underline{R}, \overline{R}\right]$ or $\hat{\mathbf{r}}(\varepsilon) = \mathbf{r}_0 + \sum_i \varepsilon_i \mathbf{r}_i$.

Because reachability analysis is performed with sets represented as zonotopes or intervals, an adaptation of the affine forms is necessary. The affine form is converted to the zonotope $\widetilde{\mathbf{r}} = \{\hat{\mathbf{r}}(\varepsilon) \,|\varepsilon_i \in [-1; 1]\}$ with $\mathbf{r}_0$ pointing to the center and $\mathbf{r}_i$ referring to the generators.

The computation with parameter variation models results in semi-symbolic HA in form of state-space equations:

$$\begin{aligned} \dot{\mathbf{x}}(t) &= \mathbf{A}\mathbf{x}(t) + \mathbf{B}\mathbf{u}(t) \\ \mathbf{y}(t) &= \mathbf{C}\mathbf{x}(t) + \mathbf{D}\mathbf{u}(t) \end{aligned} \tag{5}$$

with **A**, **B**, **C** and **D** as the state, input, output and feedthrough matrices and $\mathbf{x}(t)$ and $\mathbf{u}(t)$ are the current state vector and the source vector at time t. Every linear region of the PWL model results in an extra state-space equation. The HA model is a set of these equations. The state-space equations consist of state equations $\dot{\mathbf{x}}(t)$ and output equations $\mathbf{y}(t)$. The output equation of the first linear region is the input of the state equation in the second linear region.

Generation of PWL models leads to additional controlled sources. For parameter variation of PWL models these sources $\widetilde{i}$ and $\widetilde{u}$ are included as zonotopes in $\mathbf{y}(t)$.

3. Reduction of overapproximation

The generated semi-symbolic hybrid automata models contain intervals and affine forms, respectively. Inserting parameter variation values in these models, respectively and performing reachability analysis leads to different reachable sets, as we have shown in work [9]. Models with affine forms result mostly, but not in all cases in lower overapproximation. To reduce the overapproximation, it is necessary to determine the intersecting set of the computed reachable sets with both modeling using intervals and modeling with affine forms.

The size of the obtained reachable set after performing reachability analysis can be measured in two ways. In [17] a volume formula for zonotopes in multidimensional space is described. The other way of size measuring is to estimate the total area by calculating the projected area of all enclosed zonotopes of the reachable set. For purposes of illustration we use the latter one in this paper.

In the following we denote the total area of the reachable set by modeling with intervals as $\mathscr{A}_{Interval}$ and the total area obtained by models with affine forms as $\mathscr{A}_{AffineForms}$. The area of the intersecting set is defined as

$$\mathscr{A} = \mathscr{A}_{Interval} \cap \mathscr{A}_{AffineForms} \tag{6}$$

Possible states in the state space can only occur in the intersecting set between both reached sets. Since both methods yield overapproximation it is obvious that the area outside $\mathscr{A}$ can be reduced. Neglectable overapproximation is described as $\mathscr{A}_{Neg} = \mathscr{A}_{Interval} \Delta \mathscr{A}_{AffineForms}$. We enhance the modeling framework presented in Section 2 with Eq. (6). After automatically generating the semi-symbolic hybrid automata models and performing reachability analysis, we reduce the overapproximative reachable set, resulting in an optimized model.

Performing set operations on zonotopes will introduce additional overapproximation, thus the set operations are done with polytopes. The projected reachable sets are converted from zonotopes into polytopes. The conversion and subsequent set operations with polytopes are without additional overapproximation. The percentual area reduction is calculated as $\mathscr{A}_{Red\%} = \frac{\mathscr{A}_{Total} - \mathscr{A}_{Neg}}{\mathscr{A}_{Total}}$ with the total area of both set $\mathscr{A}_{Total} = \mathscr{A}_{Interval} \cup \mathscr{A}_{AffineForms}$. In the following, we call models with overapproximation $\mathscr{A}_{Total}$ as Model A and the optimized models containing only $\mathscr{A}$ as Model B.

4. Experimental results

Our approach is demonstrated on three circuit examples, a DC-DC converter with a D1N4148 diode shown in Fig. 3(a), a two stage nonlinear transmission line (NLTL2) circuit with D1N4148 diodes as well, shown in Fig. 3(b), and a second-order low-pass filter (LPF) with an operational amplifier LMC6484 depicted in Fig. 3(c). The PWL model of

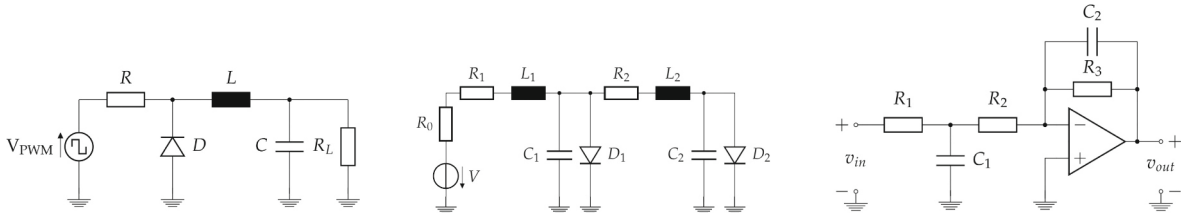

(a) DC-DC converter with LC-Filter (b) Nonlinear transmission line with two stages (NLTL2) (c) Second-order low-pass filter (LPF)

Fig. 3. Schematics of exemplary circuits.

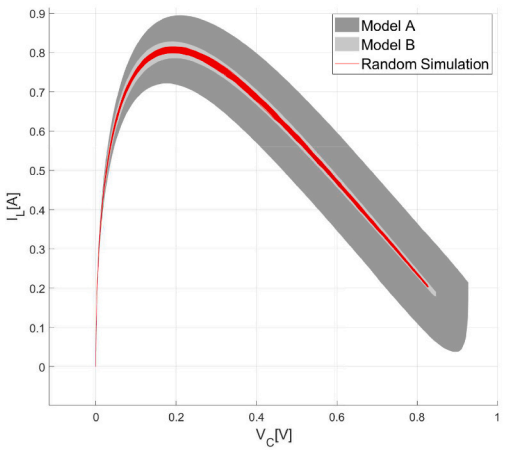

(a) DC-DC converter

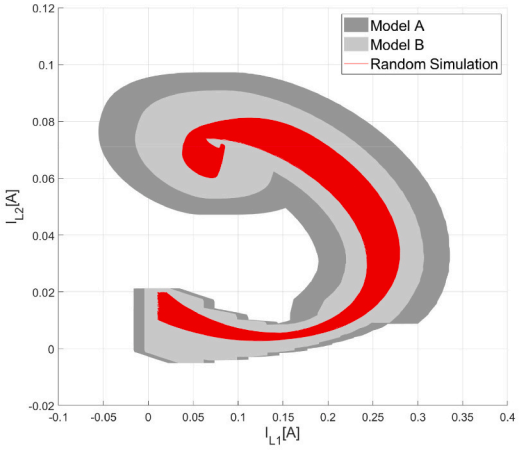

(b) NLTL2-1

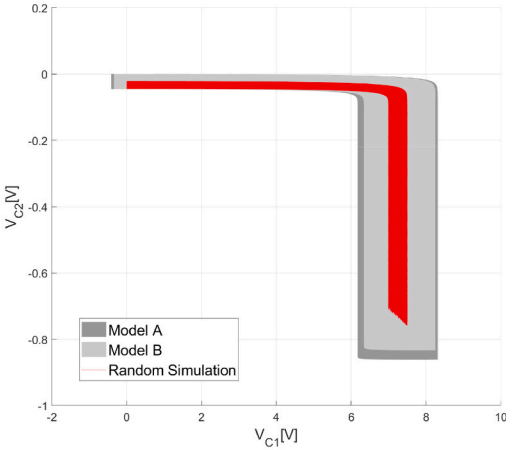

(c) LPF

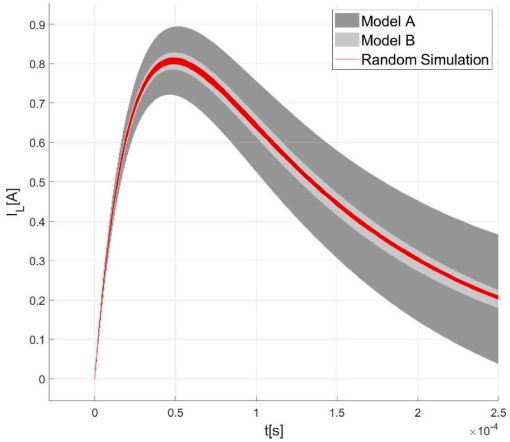

(d) Time plot of the DC-DC converter

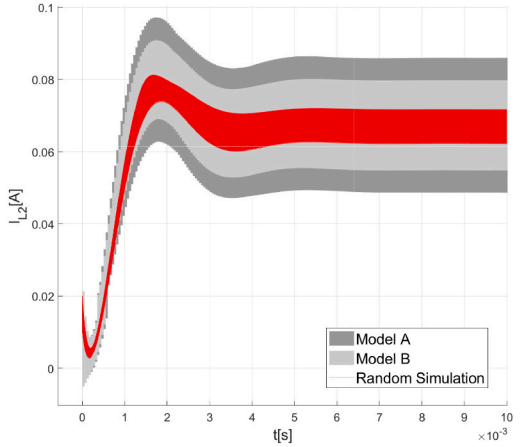

(e) Time plot of the NLTL2-1

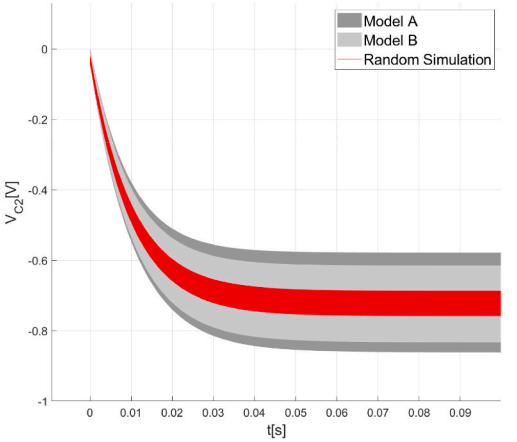

(f) Time plot of the LPF

Fig. 4. Reachable set of the exemplary circuits with parameter variations with $\mathscr{A}_{Interval} \cup \mathscr{A}_{AffineForms}$ as Model A and $\mathscr{A}_{Interval} \cap \mathscr{A}_{AffineForms}$ as Model B.

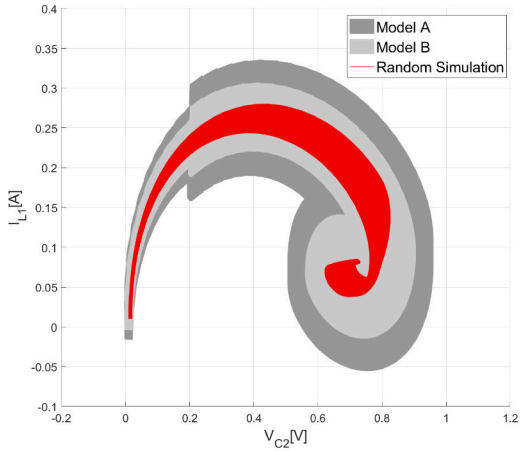

(a) NLTL2-1

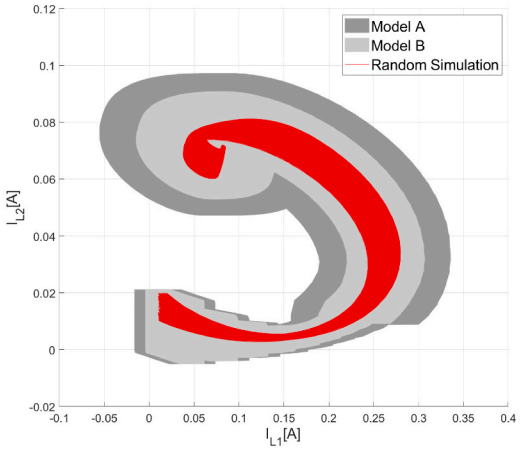

(b) NLTL2-1

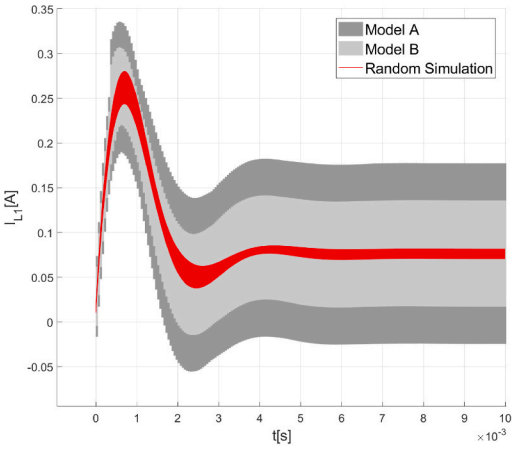

(c) Time plot of the NLTL2-1

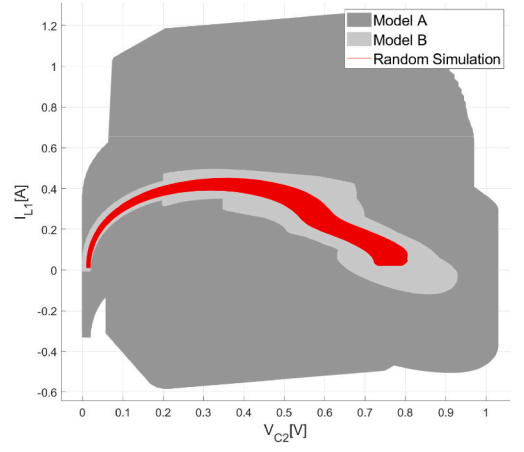

(d) NLTL2-2

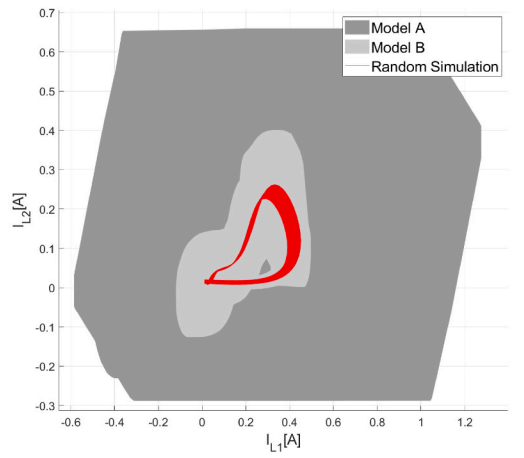

(e) NLTL2-2

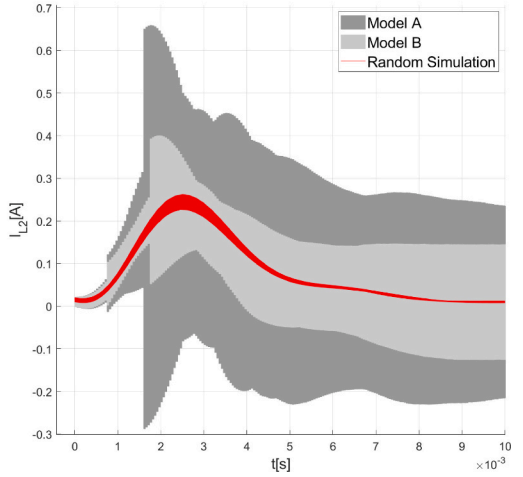

(f) Time plot of the NLTL2-2

Fig. 5. Reachable set of the circuit NLTL2 with different parameter settings with $\mathscr{A}_{Interval} \cup \mathscr{A}_{AffineForms}$ as Model A and $\mathscr{A}_{Interval} \cap \mathscr{A}_{AffineForms}$ as Model B.

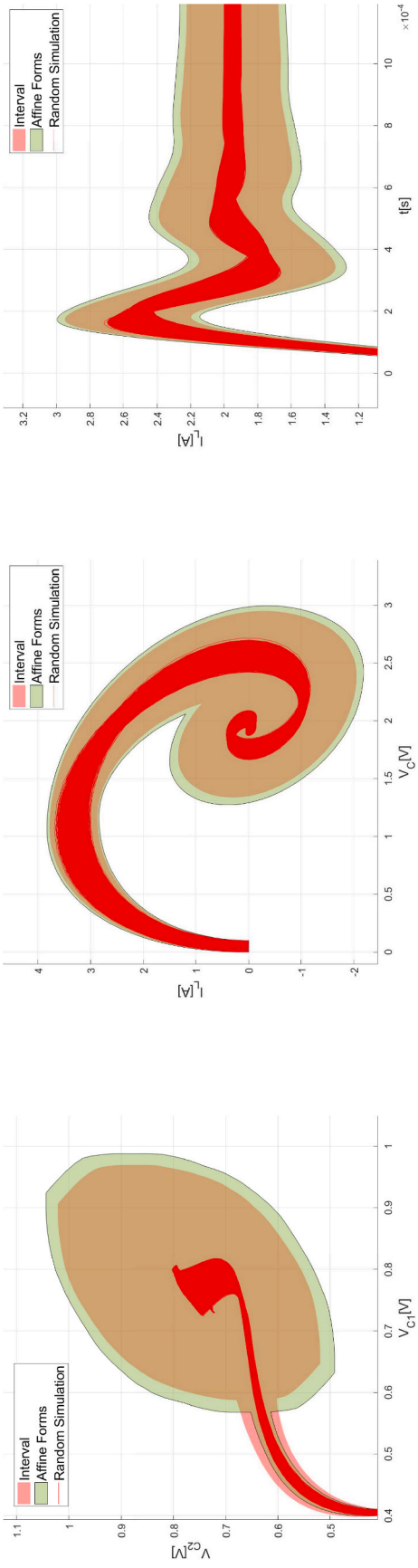

(a) NLTL2-2 with modified parameter settings (b) DC-DC converter with modified parameter settings (c) Time plot of the DC-DC converter with modified parameter settings

Fig. 6. Reachable set of the exemplary circuits with parameter variations with modeling with intervals and affine forms.

Table 1
Comparison of projected area for NLTL2–2.

Projected sizes	Projected area			
	Affine forms	Interval	Model A	Model B
V_{C1} and V_{C2}	0,1817	0,1571	0,1869	0,1519
V_{C1} and I_{L1}	0,1508	0,5142	0,5162	0,1488
t and V_{C1}	0,0027	0,0027	0,0028	0,0026
t and V_{C2}	0,0033	0,0034	0,0035	0,0032

Table 2
Comparison of runtime.

Example	Runtime[s]		
	Interval	Affine forms	Random simulation
NLTL2-1	4,4	4,0	2034,5
NLTL2-2	2,8	7,3	1125,8
DC-DC converter	1,6	1,8	16260,4
LPF	6,4	5,6	657,7

the diode consists of four linear regions and the PWL model of the operational amplifier of six linear regions. The digital parts of the AMS circuits are not explicitly shown in the schematics, but are modeled as input signals.

The specific parameter selection indicates high nonlinearity, as illustrated in Fig. 2. A closer view on the simulation of the circuit LPF shows oscillations.

Reachability analysis and simulations are performed with the software tool COntinuous Reachability Analyzer (CORA) [18]. In the following, all trajectories in the figures are obtained by simulations of the PWL model. In previous work [19,20] it has been established that the simulation trajectories are equivalent between the real model and PWL model.

In circuit LPF, the resistors are set to $R_1 = 10\ \Omega$, $R_2 = 10\ \text{k}\Omega$, and $R_3 = 1\ \text{k}\Omega$, while the capacitors are set to $C_1 = 10\ \mu\text{F}$ and $C_2 = 10\ \mu\text{F}$. Fig. 4(c) shows the reachable set of the LPF. The parameter variation is set to $\pm 1\%$ for R_2 and R_3 respectively. The initial set of the LPF has the size of 1×10^{-4} for all dimensions in $\mathbf{y}(t)$ and the input of 7.25 V with the input variation of ± 0.25 V. The reachable set is projected onto V_{C1} and V_{C2} in Fig. 4(c) and onto t and V_{C2} in Fig. 4(f). Model A and Model B reliably enclose numerous random simulation runs (red trajectories) with the same device parameter variation. Modeling errors and the input variation are as well enclosed. Model B shows a tighter enclosure of the simulation results than Model A. The reduced overapproximation with Model B amounts 26% in Fig. 4(c).

Similar results shows the next example DC-DC converter. The circuit parameters of the DC-DC converter are set to $R = 1\ \Omega$, $R_L = 100\ \Omega$, $L = 20\ \mu\text{H}$ and $C = 150\ \mu\text{F}$, respectively. The initial set has the size of 1×10^{-9} for all dimensions in $\mathbf{y}(t)$. The input signal is pulsed from 0 V to 1 V. The device parameter variation is $\pm 2\%$ for R, L and C respectively. The reachable set is projected onto V_C and I_L in Fig. 4(a) and onto t and I_L in Fig. 4(d). Model A and Model B enclose all simulation runs. Model B encloses the simulation results much tighter than Model A. The reduced overapproximation with Model B even reaches 84% in Fig. 4(a).

The results are reinforced with the third example. The reduction of overapproximation is 39% in Fig. 4(b). The circuit parameters of the NLTL2–1 are set to $R_0 = 1\ \Omega$, $R_1 = 0.5\ \Omega$, $R_2 = 10\ \Omega$, $L_1 = L_2 = 1$ mH and $C_1 = C_2 = 300$ mF. The parameter variation is set to $\pm 1\%$ for R_0, R_1 and R_2, respectively. The initial set of the NLTL2 circuit has the size of 0.01 for all dimensions in $\mathbf{y}(t)$. The input of 0.8 V with the input variation of ± 0.05 V exceeds the forward voltage of 0.7 V of the diode D1N4148.

The reachable sets of NLTL2–1 are moreover shown in Fig. 5(a) to (c). The reachable set is projected onto V_{C2} and I_{L1} in Fig. 5(a), onto I_{L1} and I_{L2} in Fig. 5(b) and onto t and I_{L1} in Fig. 5(c).

Results with another setting NLTL2–2 are illustrated in Fig. 5(d) to (f). The reachable set is projected onto the same dimensions as Fig. 5(a) to (c). The circuit parameters in this example are set to $R_0 = 0.1\ \Omega$, $R_1 = R_2 = 1\ \Omega$, $L_1 = L_2 = 1$ mH and $C_1 = C_2 = 1$ mF.

The Fig. 5(a) to (f) show the nonlinear behavior of NLTL2 with different parameter settings. The enclosure to cover the simulation results of Model B is much closer than that of Model A. The reduced overapproximation of the reachable set with Model B gains up to 41% in Fig. 5(a) with the first parameter setting and even up to 86% in Fig. 5(d) with the second parameter setting.

The analyses show that Model B consistently has a significantly lower overapproximation. Considered more closely, in most cases models with affine forms are a subset of models with intervals. The effect grows with higher nonlinearity and the increasing number of calculation steps.

There are cases, in which the reachable set $\mathscr{A}_{AffineForms}$ using models with affine forms overlaps the set $\mathscr{A}_{Interval}$ using intervals in some places, shown in Fig. 6. This means, the set difference $\mathscr{A}_{Neg} = \mathscr{A}_{Interval} \Delta \mathscr{A}_{AffineForms}$ is not empty.

The presented results in Fig. 6 have a resonant circuit in common, which oscillates with damping and reaches the stable state. Here, the initial set of the modified NLTL2–2 circuit has the size of 0.005 for all dimensions in $\mathbf{y}(t)$ and the center in 0.405. The modified settings of the DC-DC converter example are $R = 0.25\ \Omega$, the initial set with the size of 0.05 for all dimensions in $\mathbf{y}(t)$ and the parameter variation is set to $\pm 20\%$ for C. The input signal is pulsed from 0 V to 1.95 V with the input variation of ± 0.05 V. Here, the PWL model of the diode consists of eight linear regions.

Table 1 shows the area results of the example NLTL2–2. Depending on the projected sizes and parameter settings models with affine forms or models with intervals may prove more appropriate. This consideration illustrates the importance of generating the subset Model B, because the result is unknown beforehand. With Model B an additional reduction in overapproximation with around 3% compared to the more appropriate model is achieved.

Table 2 shows the average runtime results of the examples. The runtime of Random simulation consists of 1000 trajectory runs. All computations are performed on a 64 bit system with an Intel i7-2600K processor at 3.4 GHz and 16 GB RAM. The modeling approach not only offers reliable results, but also enables an acceptable runtime.

5. Conclusion

In this paper, we have presented an approach, which generates reliable AMS circuit models with a highly reduced overapproximation. In all cases simulation runs with variations of different parameter were fully enclosed of the generated models. We have shown that this approach is applicable on circuit examples with highly nonlinear behavior. The reduction of overapproximation on the demonstrated examples reaches up to 86%.

CRediT authorship contribution statement

Malgorzata Rechmal-Lesse: Conceptualization, Methodology, Writing - Original Draft, Writing - Review & Editing, Investigation, Visualization.

Yeremia Gunawan Adhisantoso: Software, Validation, Investigation, Visualization.

Gerald Alexander Koroa: Software, Validation, Investigation, Visualization.

Markus Olbrich: Supervision.

Declaration of competing interest

The authors declare that they have no known competing financial interests or personal relationships that could have appeared to influence the work reported in this paper.

Acknowledgment

This work was partially funded by the Deutsche Forschungsgemeinschaft (DFG – German Research Foundation) under project faveAC under grant OL 121/4-1.

References

[1] D. Grabowski, M. Olbrich, E. Barke, Analog circuit simulation using range arithmetics, in: 2008 *Asia and South Pacific Design Automation Conference*, IEEE, 2008, pp. 762–767.
[2] A. Krause, M. Olbrich, E. Barke, Enclosing the modeling error in analog behavioral models using neural networks and affine arithmetic, in: 2012 International Conference on Synthesis, Modeling, Analysis and Simulation Methods and Applications to Circuit Design (SMACD), IEEE, 2012, pp. 5–8.
[3] C. Zivkovic, C. Grimm, M. Olbrich, O. Scharf, E. Barke, Hierarchical verification of ams systems with affine arithmetic decision diagrams, IEEE Transactions on Computer-Aided Design of Integrated Circuits and Systems 38 (10) (2018) 1785–1798.
[4] H. Lin, P. Li, C.J. Myers, Verification of digitally-intensive analog circuits via kernel ridge regression and hybrid reachability analysis, in: 2013 50th ACM/EDAC/IEEE Design Automation Conference (DAC), IEEE, 2013, pp. 1–6.
[5] T. Dang, A. Donzé, O. Maler, Verification of analog and mixed-signal circuits using hybrid system techniques, in: International Conference on Formal Methods in Computer-Aided Design, Springer, 2004, pp. 21–36.
[6] N. Kochdumper, A. Tarraf, M. Rechmal, M. Olbrich, L. Hedrich, M. Althoff, Establishing reachset conformance for the formal analysis of analog circuits, in: 2020 25th Asia and South Pacific Design Automation Conference (ASP-DAC), IEEE, 2020, pp. 199–204.
[7] M. Althoff, O. Stursberg, M. Buss, Reachability analysis of linear systems with uncertain parameters and inputs, in: 2007 46th IEEE Conference on Decision and Control, IEEE, 2007, pp. 726–732.
[8] O.A. Beg, H. Abbas, T.T. Johnson, A. Davoudi, Model validation of pwm dc–dc converters, IEEE Trans. Ind. Electron. 64 (9) (2017) 7049–7059.
[9] M. Rechmal-Lesse, G.A. Koroa, Y.G. Adhisantoso, M. Olbrich, Automatically generated nonlinear analog circuit models enclosing variations with intervals and affine forms for reachability analysis, in: 2020 23rd International Symposium on Design and Diagnostics of Electronic Circuits & Systems (DDECS), IEEE, 2020, pp. 1–4.
[10] W.M.G. van Bokhoven, Piecewise-Linear Modelling and Analysis, Kluwer Technische Boeken Deventer, The Netherlands, 1981.
[11] R. Killick, P. Fearnhead, I.A. Eckley, Optimal detection of changepoints with a linear computational cost, J. Am. Stat. Assoc. 107 (500) (2012) 1590–1598.
[12] C.-W. Ho, A. Ruehli, P. Brennan, The modified nodal approach to network analysis, IEEE Transactions on circuits and systems 22 (6) (1975) 504–509.
[13] S. Natarajan, A systematic method for obtaining state equations using mna, IEE Proceedings G-Circuits, Devices and Systems 138 (3) (1991) 341–346.
[14] S. Hoelldampf, H.-S. Lee, D. Zaum, M. Olbrich, E. Barke, Efficient generation of analog circuit models for accelerated mixed-signal simulation, in: 2012 IEEE International SOC Conference, IEEE, 2012, pp. 104–109.
[15] H.-S.L. Lee, M. Althoff, S. Hoelldampf, M. Olbrich, E. Barke, Automated generation of hybrid system models for reachability analysis of nonlinear analog circuits, in: The 20th Asia and South Pacific Design Automation Conference, IEEE, 2015, pp. 725–730.
[16] J. Stolfi, L.H. de Figueiredo, An introduction to affine arithmetic, TEMA (São Carlos) 4 (3) (2003) 297–312.
[17] E. Gover, N. Krikorian, Determinants and the volumes of parallelotopes and zonotopes, Linear Algebra Appl. 433 (1) (2010) 28–40.
[18] M. Althoff, Cora 2016 Manual vol. 85748, TU Munich, 2016.
[19] S. Divanbeigi, H.-S. Lee, E. Roehrig, M. Olbrich, E. Barke, Modeling of linear stimuli for accelerated mixed-signal simulations, in: ANALOG 2016; 15. ITG/GMM-Symposium, VDE, 2016, pp. 1–5.
[20] S. Divanbeigi, E. Aditya, Z. Wang, M. Olbrich, Enabling complex stimuli in accelerated mixed-signal simulation, in: Proceedings of the 56th Annual Design Automation Conference 2019, 2019, pp. 1–6.